

# EFFECTS OF PULSAR ROTATION ON TIMING MEASUREMENTS OF THE DOUBLE PULSAR SYSTEM J0737-3039

Roman R. Rafikov<sup>1</sup> and Dong Lai<sup>2</sup>

Draft version February 7, 2020

## ABSTRACT

We study the effect of pulsar rotation on timing of binary pulsars, with particular emphasis on the double pulsar system J0737-3039. Special relativistic aberration due to the orbital motion of pulsar changes both the longitude and colatitude of the emission direction with respect to the pulsar spin axis. The former gives rise to a shift of the arrival time of the pulse centroid (this is the conventional "longitudinal" aberration delay), the latter results in a distortion (contraction or dilation) of the pulse profile on the orbital time scale. The amplitude of pulse distortion depends inversely on the variation of polarization position angle across the pulse. For small angle between the pulsar magnetic and spin axes, as inferred for PSR J0737-3039A from polarimetric observations, the pulse distortion is significant (~1%) and the associated "latitudinal" aberration delay is much larger than the longitudinal one. We show that by monitoring the arrival time of separate pulse components as a function of pulsar orbital phase, the latitudinal aberration delay may be easily measured with the current timing precision. Such measurement would constrain the spin geometry of the system. The latitudinal delay can also be detected by monitoring system's orbital parameters on the geodetic precession time scale. Because of the near edge-on orbital orientation of the PSR J0737-3039 system, general relativistic bending of pulsar A's radio beam near its superior conjunction also introduces spin-dependent time delays of similar order of magnitude as the aberration delays. In addition, light bending splits the pulse profile into two variable components, corresponding to two gravitationally lensed images of the source. Detection of lensing effects is challenging, but may be possible with existing technology.

Subject headings: pulsars: general | stars: neutron | pulsars: individual (J0737-3039A, J0737-3039B) | gravitational lensing | binaries: general

## 1. introduction

The recently discovered double pulsar system J0737-3039 (Burgay et al. 2003; Lyne et al. 2004) presents an unprecedented natural laboratory for testing our understanding of general relativity and pulsar magnetosphere physics. One of the unique features of this system is the almost edge-on orientation of its orbital plane with respect to our line of sight. Currently the two best constraints on the system's inclination come from the Shapiro delay ( $i = 88.7 \pm 0.9$ ; Lyne et al. 2004; Ransom et al. 2004) and from scintillation measurements ( $i = 90.29 \pm 0.14$ , Coles et al. 2004). Among other effects this high inclination leads to periodic eclipses of the millisecond pulsar (pulsar A) by plasma in the magnetosphere of the normal pulsar (pulsar B) (see Lyne et al. 2004; Kaspi et al. 2004; McLaughlin et al. 2004; Arons et al. 2004; Rakhov & Goldreich 2004; Lyutikov & Thompson 2005).

The edge-on orientation of the system also makes possible gravitational light bending of the pulsar signal when the pulsar passes through its superior conjunction with respect to the companion. In Lai & Rafikov (2005), we studied the effect of gravitational lensing on the pulse intensity and the impact of light bending on the correlated scintillation measurements of both pulsars. We also evaluated the effects of light bending on the pulse arrival time: geometric time delay and the modified Shapiro delay | both of these timing contributions are independent

of the pulsar spin.

Since pulsar signals are due to the beamed emission of a rotating neutron star (as opposed to radial pulsation of the star), additional spin-dependent time delays arise due to special relativistic aberration (Shapiro & Blandford 1976; Damour & Deruelle 1986) and general relativistic light bending (cf. Schneider 1990). The goal of this paper is to evaluate these spin-dependent delays in the PSR J0737-3039 system, and assess their detectability and potential for constraining the parameters of the system. We also examine the distortion of pulse profile due to aberration and lensing, and discuss an alternative way of analyzing pulse arrival time and introduce the concept of "latitudinal delay" that focuses on specific features in the pulse profile. For PSR J0737-3039, a measurement of this latitudinal delay may lead to useful constraints on the geometry of the system.

In x2, we calculate the spin-dependent time delays due to aberration and lensing. In x3, we examine the pulse shape distortion/variation and calculate the latitudinal delays. The prospects of detecting these effects are discussed in x4.

Although the formulae derived in this paper are general for any binary pulsar system, we shall apply them to PSR J0737-3039, concentrating on the effects of rotational delays on the timing of the millisecond pulsar A, with pulsar B playing the role of the lensing companion. We adopt the following parameters for the system:  $M_p = M_A = 1.337M_\odot$ ;  $M_c = M_B = 1.25M_\odot$ , the spin period of pulsar A  $P_A = 22.7$  ms, the orbital period  $P_b = 0.1023$  d, the orbital semimajor axis  $a = 8.784 \times 10^{10}$  cm, eccentricity  $e = 0.0878$ , longitude

<sup>1</sup>IAS, Einstein Drive, Princeton, NJ 08540; rrr@ias.edu

<sup>2</sup>Department of Astronomy, Cornell University, Ithaca, NY 14853; dong@astro.cornell.edu

of periastron  $\tau = 73.8$  (as of 2004), and the orbital inclination angle  $i$  in the range between  $90.14^\circ$  and  $90.56^\circ$ .

## 2. spin-dependent time delays

Because of special relativistic light aberration, the direction of emission in the comoving frame of the pulsar,  $\mathbf{N}$  ( $\mathbf{N} \cdot \mathbf{j} = 1$ ), differs from that in the observer's frame,  $\mathbf{n}$  ( $\mathbf{n} \cdot \mathbf{j} = 1$ ), by the vector

$$(\mathbf{n})_A = \mathbf{n} - (\mathbf{n} \cdot \mathbf{v}_p) \mathbf{n}_0 - (\mathbf{n}_0 \cdot \mathbf{v}_p) \mathbf{n}_0; \quad (1)$$

where  $\mathbf{v}_p = c \mathbf{v}_p$  is the pulsar velocity relative to the binary barycenter<sup>3</sup>, and  $\mathbf{n}_0$  is the unit vector from the binary system to the observer. Because of general relativistic light bending, the direction of emission  $\mathbf{n}$  at the pulsar position differs from  $\mathbf{n}_0$ . This lensing effect is important only around the superior conjunction of the pulsar, with the deflection vector  $(\mathbf{n})_L = \mathbf{n} - \mathbf{n}_0$  given by

$$(\mathbf{n})_L = \frac{\mathbf{R}}{R_s} - \frac{\mathbf{R}_s}{a_k} = \frac{\mathbf{R}}{R_s} - \frac{\mathbf{n}_0 \cdot (\mathbf{r} - \mathbf{r}_0)}{a_k}; \quad (2)$$

Here  $\mathbf{r} = \mathbf{r}_p$ ,  $\mathbf{r}_0$  is the position vector of the pulsar relative to its companion,  $R_s = \mathbf{n}_0 \cdot (\mathbf{r} - \mathbf{r}_0)$  is the projection of  $\mathbf{r}$  in the sky plane,  $R_s = \mathbf{R}_s \mathbf{j} = \mathbf{r}(1 - \sin^2 i \sin^2 \iota)^{1/2}$  ( $\iota$  is the true anomaly measured from the ascending node of the pulsar), and  $a_k = \sin i(1 - \epsilon^2) = (1 + e \sin \tau)^{-1}$  is the distance projected along our line of sight between the pulsar and its companion at the conjunction ( $a$ ,  $e$  and  $\tau$  are the orbital semi-major axis, eccentricity, and longitude of periastron, respectively). Gravitational lensing gives rise to two pulsar images (specified by the subscript "\prime");  $\mathbf{R}$  is the displacement (in the sky plane) of the image position,  $R = (R = R_s + 1)R_s$ , relative to the fiducial position,  $R_s$ , and is given by

$$R = \frac{1}{2} \frac{q}{R_s^2 + 4R_E^2} R_s; \quad (3)$$

with the Einstein radius

$$R_E = (2R_g a_k)^{1/2}, \quad (2R_g a)^{1/2} = 2550 \text{ km}; \quad (4)$$

Here  $R_g = 2GM/c^2 = 3.69 \text{ km}$  and the numerical value is for J0737-3039A with pulsar B playing role of the companion. Combining eqs. (1) and (2), the direction of emission in the pulsar's comoving frame is  $\mathbf{N} = \mathbf{n}_0 + \mathbf{N}$ , with  $\mathbf{N} = (\mathbf{n})_A + (\mathbf{n})_L$ . The deflection angle of the emission vector due to light bending,  $\mathbf{R} = \mathbf{a}$ , has a maximum value (for the "plus" image)  $R_E = a \sqrt{v/c}$  (this occurs at the orbital conjunction and  $i = 90^\circ$ ), which is of the same order as the aberration effect.

Variation of the emission direction  $\mathbf{N}$  causes a shift in the equatorial longitude of  $\mathbf{N}$  in the corotating frame of pulsar (counted in the direction of rotation) given by

$$= \frac{\mathbf{N} \cdot (\mathbf{s} \cdot \mathbf{n}_0)}{\mathbf{s}_p \cdot \mathbf{n}_0^2}; \quad (5)$$

where  $\mathbf{s}_p$  is the unit vector along the pulsar spin axis. For an arbitrary emission pattern rigidly rotating around  $\mathbf{s}_p$ , any change in the equatorial longitude corresponds to a change of emission phase, leading to a time delay

<sup>3</sup> The constant velocity of the barycenter itself does not affect timing measurement.

$t = t_p = (t)_A + (t)_L$  (here  $t_p$  is the angular frequency of the pulsar and the time delay is positive for signal arriving later), where

$$(t)_A = \frac{p}{p \mathbf{v}_p} \frac{(\mathbf{s} \cdot \mathbf{n}_0)}{\mathbf{n}_0^2}; \quad (6)$$

$$(t)_L = \frac{\mathbf{R}}{R_s} - \frac{\mathbf{r} \cdot (\mathbf{s} \cdot \mathbf{n}_0)}{p a_k \mathbf{v}_p \mathbf{n}_0^2} \quad (7)$$

are contributions due to aberration (Smart & Braden 1975) and gravitational light bending (cf. Schneider 1990), respectively. Note that this "longitudinal" time delay shifts the whole pulse profile uniformly without introducing any distortions to its shape (see x3).

The pulsar spin axis  $\mathbf{s}_p$  is specified by two angles:  $\alpha$  is the angle between  $\mathbf{s}_p$  and the light-of-sight vector  $\mathbf{n}_0$ ,  $\beta$  is the angle between the ascending node of the orbit and the projection of  $\mathbf{s}_p$  on the sky plane. The aberration time delay (6) is then given by

$$(t)_A = A (\sin \alpha + e \sin \tau) + B (\cos \alpha + e \cos \tau); \quad (8)$$

with

$$\frac{A}{B} = \frac{p \frac{b a_p}{c}}{1 - \epsilon^2 \sin \alpha} \frac{\sin \alpha}{\cos \alpha \cos \beta}; \quad (9)$$

where  $b = (GM/c^3)^{1/2}$ ,  $M_t = M_p + M_c$  is the total mass of the system, and  $a_p = (M_c/M_t)a$ . These expressions coincide with the results of Damour & Deruelle (1986). Similarly, the delay associated with light bending is<sup>4</sup>

$$(t)_L = \frac{\mathbf{R}}{R_s} - \frac{\mathbf{r}}{a_k} - \frac{\sin \alpha \cos \beta}{p \sin \alpha} \frac{\cos \alpha \cos \beta}{p \sin \beta} + \frac{(\sin \alpha \cos \beta - \cos \alpha \cos \beta)}{\sin \alpha (1 - \sin^2 i \sin^2 \iota)^{1/2}}; \quad (10)$$

where  $\mathbf{r} = a(1 - \epsilon^2) = (1 + e \cos \tau)$  ( $\iota = \iota_0 + \tau$  is the orbital true anomaly measured from periastron). Note that the lensing effect is important only around the orbital conjunction ( $\iota = \iota_0 = 180^\circ$ ) for nearly edge-on systems. Let  $i = 90^\circ$  and  $\iota = 180^\circ$ , with  $j = j_0 + \tau$ , then we have

$$(t)_L' = \frac{\mathbf{R}}{a_k p} \frac{i \cos \beta}{\sin \beta} \frac{\sin \alpha}{[(i - j)^2 + (\iota - \iota_0)^2]^{1/2}}; \quad (11)$$

with  $\mathbf{R}$  given by eq. (3) and  $R_s = \sqrt{a_k^2 + (i - j)^2 + (\iota - \iota_0)^2}$ .

Neglecting the dependence on various angles, the aberration time delay is of order  $b a_p = (c v_p) = 3.6 \text{ s}$ , and the rotational lensing delay at the conjunction is of order  $R = (a_k p) = 10.5 (R = R_E) \text{ s}$ . Not surprisingly, the two delays are of the same order of magnitude at the conjunction, since  $b a_p = v/c = (2c)$  and  $R_E = a \sqrt{v/c} = 2v/c$ .

<sup>4</sup> This agrees with expression of Schneider (1990) if we replace  $a_k$  by  $r \mathbf{v}_p = r \sin i \sin \beta$  (this would lead to divergence at  $i = 0^\circ$ ). Note the eq. (10) disagrees with the result of Doroshenko & Kopeikin (1995), which, in their interpretation, does not involve Einstein radius at all. Also note that some previous treatments of the light bending delays (Schneider 1990; Doroshenko & Kopeikin 1995; Góicoechea et al. 1995) were restricted to circular or purely edge-on orbits.

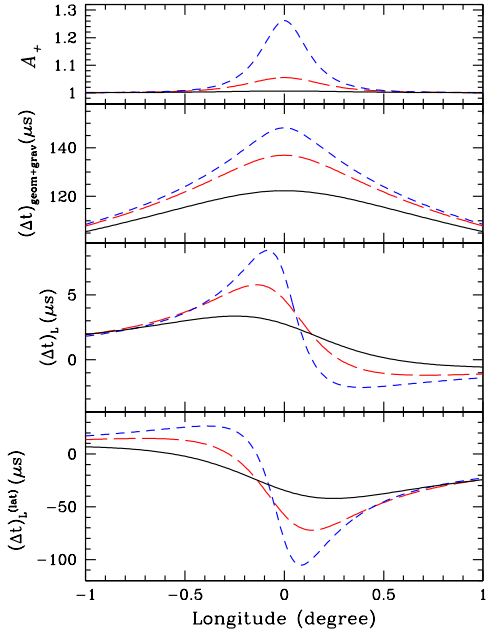


Fig. 1. The amplification (top panel), the combined geometric and gravitational (Shapiro) delay (the second panel), the rotational lensing delay (the third panel), and the latitudinal lensing delay (the bottom panel) of the dominant ('plus') in age of the pulsar A signal as a function of the orbital phase. The longitude is measured from the superior conjunction of pulsar A (when A is exactly behind pulsar B). In each panel, the inclination angles are  $i = 90:56$  (solid line),  $90:28$  (long-dashed line) and  $90:14$  (short-dashed line). For the third and bottom panels, the angles  $\alpha = 50^\circ$ ,  $\beta = 45^\circ$  and  $\tan \delta = 0:08$  are used.

Damour and Deruelle (1986) recognized that the aberration delay is degenerate with the Römer delay, and therefore cannot be directly measured (but see x4). The time delays associated with lensing do not suffer from this degeneracy. Figures 1 and 2 show these delays (the combined geometric and Shapiro delays as calculated in Lai & Rakov (2005), and the rotational lensing delay given by eq. [10] or [11]) together with the amplification factor for both in ages,

$$A = \frac{u^2 + 2}{2u} \frac{1}{u^2 + 4} \quad \frac{1}{2}; \quad u = R_s/R_E : \quad (12)$$

In evaluating  $(\Delta t)_L$ , we adopt  $\alpha = 50^\circ$  as suggested by Demorest et al. (2004) from polarization measurement (although this angle is currently unconstrained) and use  $\beta = 45^\circ$  as an example in Figures 1 and 2. The magnitude of  $(\Delta t)_L$  scales as  $(\sin i)^{-1}$  and its shape depends on  $\delta$  as  $(i) \cos \delta - (L) \sin \delta$ . Unlike the geometric delay and Shapiro delay, the rotational lensing delay is generally asymmetric with respect to orbital conjunction (the exception is when  $\delta = 0^\circ, 180^\circ$ ). Note that although the delays associated with the 'minus' in age can become very large (100's of s) as a result of its large deflection ( $\beta R = a_k$ ), this in age is usually too demagnified to be of interest (see x3.3).

### 3. pulse profile variation and \latitudinal time delay"

#### 3.1. Pulse Profile Variation

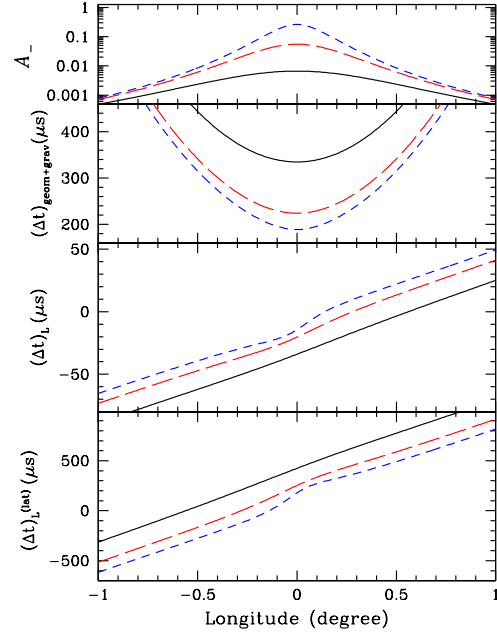


Fig. 2. Same as Figure 1, except for the subdominant ('minus') in age.

Variation of the pulse emission direction  $\mathbf{N}$  also results in the change of colatitude of emission vector  $\mathbf{j}$ . Since  $\cos \delta = \mathbf{s}_p \cdot \mathbf{N}$  and  $\sin \delta = \mathbf{j} \cdot \mathbf{N}$  we find

$$= \frac{\mathbf{s}_p}{\dot{\mathbf{s}}_p} \frac{\mathbf{N}}{n_0 \mathbf{j}} = (\alpha)_A + (\alpha)_L; \quad (13)$$

where

$$\begin{aligned} (\alpha)_A &= (n_0 - \mathbf{s}_p) \frac{(\mathbf{s}_p - n_0 \mathbf{j})}{\dot{\mathbf{s}}_p - n_0 \mathbf{j}} \\ &= \frac{p}{c} \frac{b \dot{\mathbf{a}}_p}{1 - \epsilon^2} [\cos \sin (\cos + e \cos \delta)] \\ &\quad \cos (\sin + e \sin \delta)]; \end{aligned} \quad (14)$$

$$\begin{aligned} (\alpha)_L &= \frac{R}{a_k R_s} \frac{(n_0 - r)}{\dot{\mathbf{s}}_p} \frac{(\mathbf{s}_p - n_0 \mathbf{j})}{n_0 \mathbf{j}} \\ &= \frac{R}{R_s} \frac{r}{a_k} (\cos \cos + \cos \sin \sin) \end{aligned} \quad (15)$$

are the contributions from aberration and lensing, respectively.

Unlike the shift of longitude, shift of colatitude affects the different components of pulse profile differently thus changing pulse profile periodically on the orbital timescale. In the following we consider a specific radio emission pattern based on the rotating vector model (RVM; Radhakrishnan & Cooke 1969) widely used for interpreting pulsar pulse profile and polarization data. In this model, the radio emission pattern consists of a set of cones which are circular<sup>5</sup> in cross section as seen along the magnetic axis (see Fig. 3). As a result of pulsar rotation around  $\mathbf{s}_p$ , our line of sight  $\mathbf{n}_0$  passes through the

<sup>5</sup> More complicated emission patterns would change the interpretation of pulsar spin geometry as inferred from timing data but will not affect our basic conclusions; their effect can be treated similarly to that of RVM.

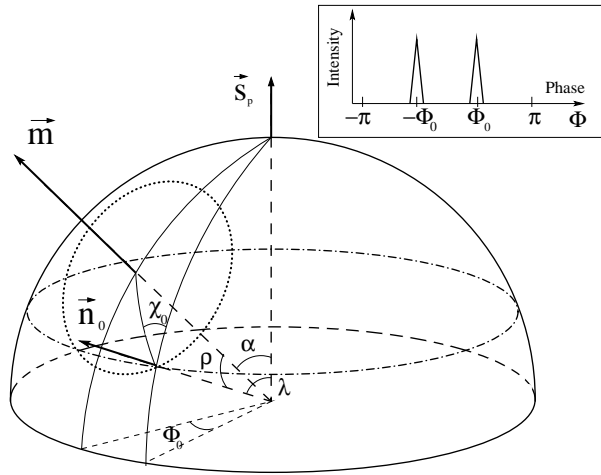


Fig. 3.1 Geomtry of pulsar emission with respect to the spin axis  $s_p$ , magnetic axis  $m$ , and our line of sight  $n_0$ . The latter cuts the celestial sphere and emission pattern (cone with opening angle  $j$ ; the dotted circle denotes its intersection with celestial sphere) along the dot-dashed line in the course of pulsar rotation, giving rise to features of the pulse profile at  $\phi_0$ , shown schematically in the inset.

emission cone with half opening angle  $\theta > j$  ( $\theta$  is the angle between  $s_p$  and  $m$ ) which causes two episodes of radio emission at the pulse phases  $\phi_0$  corresponding to the leading and trailing edges of the cone<sup>6</sup>. Emission patterns close to circular are supported by theoretical ideas of pulsar emission mechanisms and observations of slow pulsars (Rankin 1993), although their occurrence in millisecond pulsars is not so clear (Kramer et al. 1998; Weisberg & Taylor 2002). The observed pulse profile of PSR J0737-3039A is consistent with a circular emission pattern (Demorest et al. 2004; Manchester et al. 2005).

The full width of the pulse is  $2\theta_0$ , with

$$\cos \theta_0 = \frac{\cos \alpha \cos \cos}{\sin \sin} : \quad (16)$$

The variation of  $\theta_0$  then leads to a variation of  $\phi_0$ :

$$\theta_0 = \frac{1}{\tan \phi_0 \tan} \frac{1}{\sin \phi_0 \tan} : \quad (17)$$

It is easy to show that  $\phi_0$  is given by (which is also clear from Fig. 4)

$$\theta_0 = \frac{\sin \sin \phi_0}{\cos \sin \cos \phi_0 \sin \cos} : \quad (18)$$

where  $\phi_0$  is the angle (on the celestial sphere) between the arc connecting  $n_0$  and  $s_p$  and the arc connecting  $n_0$  and  $m$  at the edges of the pulse, i.e., it coincides with the position angle of linear polarization and is given by the usual expression (Komesaroff 1970)

$$\tan \phi_0 = \frac{\sin \sin \phi_0}{\cos \sin \cos \phi_0 \sin \cos} : \quad (19)$$

Equation (18) shows that the change of pulse width depends inversely on the change of position angle of radio

<sup>6</sup> Radio intensities of two emission episodes are generally different because of the complicated azimuthal structure of emitting region.

polarization across the pulse. It also shows that while is generally quite small ( $\gamma = c / 10^3$  due to aberration and  $R = a / 3 \cdot 10^3$   $R_E$  due to lensing),  $\phi_0$  can be significant when  $\sin \tan \phi_0$  is small, as in the case of the PSR J0737-3039 system (see x3.3.2).

### 3.2. Latitudinal Time Delay

Standard pulsar timing formulae (including those discussed in x2) measure the arrival time of the centroid of radio pulses. However, pulse profile often has multiple components; in the rotating vector model these components correspond to passages of  $n_0$  through different emission cones (two for each cone). As discussed above, the variation of colatitude of emission direction due to aberration and lensing results in the change of the location (in phase) of a given pulse component relative to the pulse centroid. Thus if one times the arrival of a specific component of the pulse, additional delay associated with such shift of colatitude must be included; we call this "latitudinal delay".

In the rotating vector model, the latitudinal delay associated with the leading edge of the pulse is<sup>7</sup>

$$(\Delta t)^{(\text{lat})} = \theta_0 = p = (\Delta t)_A^{(\text{lat})} + (\Delta t)_L^{(\text{lat})}; \quad (20)$$

where  $(\Delta t)_A^{(\text{lat})}$  and  $(\Delta t)_L^{(\text{lat})}$  are contributions due to aberration and lensing. Using eqs. (14) and (18), we find the latitudinal aberration delay

$$(\Delta t)_A^{(\text{lat})} = C (\sin \phi_0 + e \sin \phi_0) + D (\cos \phi_0 + e \cos \phi_0) \quad (21)$$

where

$$C = \frac{p \frac{b \bar{a} p}{c} \frac{1}{1 - \frac{e}{\sin \tan \phi_0}} \cos \phi_0}{\cos \sin \tan \phi_0} \quad (22)$$

with  $\tan \phi_0$  given by (19) in the framework of RVM. Similarly, using eq. (15), we find the latitudinal lensing delay

$$(\Delta t)_L^{(\text{lat})} = \frac{R}{R_s} \frac{r \cos \phi_0 \cos \phi_0 + \cos \sin \phi_0 \sin \phi_0}{a_k p \sin \tan \phi_0} + \frac{R}{a_k p} \frac{i \sin \phi_0 + \cos \phi_0}{\sin \tan \phi_0 [(i^2 + (1 - \frac{e}{\sin \tan \phi_0})^2)^{1/2}]}; \quad (23)$$

where the second equality comes from expansion around  $\phi_0 = -2 + i$  and  $i = -2 + \phi_0$ .

Naturally, if one times the arrival of a specific component of pulse profile, then the total delay is the sum of the longitudinal contributions [eqs. (8), (10)] associated with the shift of the pulse centroid and the latitudinal contributions [eqs. (21), (23)] associated with pulse dilation/shrinkage. Thus, the combination of longitudinal and latitudinal delays results in (1) a uniform shift of the whole pulse profile in time by  $(\Delta t)_A + (\Delta t)_L$  and (2) a nonuniform profile contraction/dilation, with each pulse component being shifted in phase by  $\phi_0 = p [(\Delta t)_A^{(\text{lat})} + (\Delta t)_L^{(\text{lat})}]$ . Pulse components closer to the pulse centroid (i.e. those with smaller  $\phi_0$ ) are relatively more susceptible to contraction/dilation than the more distant components.

<sup>7</sup> For the trailing edge, the delay is  $\theta_0 = p$ . Hereafter our formulae refer to the leading edge of the pulse.

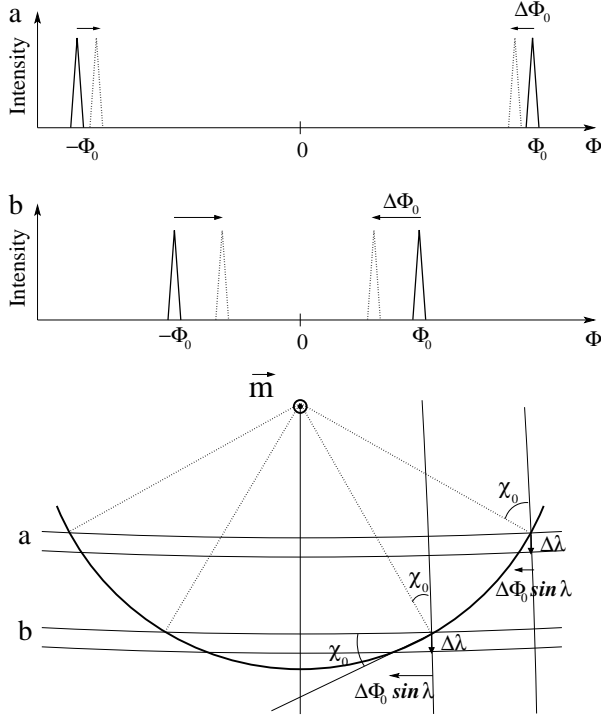


Fig. 4. | Variation of the pulse profile as a result of latitudinal variation for two different cuts of our line of sight  $n_0$  through the circular emission pattern. The bottom panel shows the projection onto the pulsar's celestial sphere along the magnetic axis: the thick solid arc depicts part of the emission cone, the thin vertical arcs represent projections of meridians, and the dotted lines denote the magnetic field lines,  $a$  and  $b$  denote the locus of two different lines of sight. This Figure illustrates how the proximity of our line of sight to the edge of the emission cone affects the total pulse width.

To evaluate  $(t)^{(\text{lat})}$ , a knowledge of  $\chi_0$  and  $\lambda$  is necessary. Analysis of polarization data of PSR J0737-3039A constrains the angle between the spin axis and the magnetic axis to be  $\sim 4^\circ$ , while leaving unconstrained (Demorest et al. 2004). Based on the opening angle of other millisecond pulsars and  $\sim 4^\circ$ , Demorest et al. (2004) suggests  $\sim 50^\circ$ , which we adopt in our estimate. The pulse profile of pulsar A exhibits remarkable similarity between its outermost leading and trailing edges (Demorest et al. 2004; Manchester et al. 2005) at  $\chi_0 \approx 115^\circ$ , which suggests that all profile components come from the same magnetic pole and that the two prominent spikes in the pulse profile can be associated with leading and trailing edges of the same emission cone. Equation (19) then yields  $\tan \chi_0 \approx 0.08$ . The bottom panels of Figures 1 and 2 depict the lensing latitudinal delay  $(t)_L^{(\text{lat})}$  for both images. Clearly, because of the small value of  $\tan \chi_0$  for the PSR J0737 system,  $(t)_L^{(\text{lat})}$  is much larger than  $(t)_L$ .

### 3.3. Effect of Double Images

In addition to the pulse profile change due to the change of emission colatitude (see x3.1), gravitational lensing affects pulse profile in another way. Near the orbital conjunction, light bending splits the source (pulsar) into two radio images in the plane of the sky. The

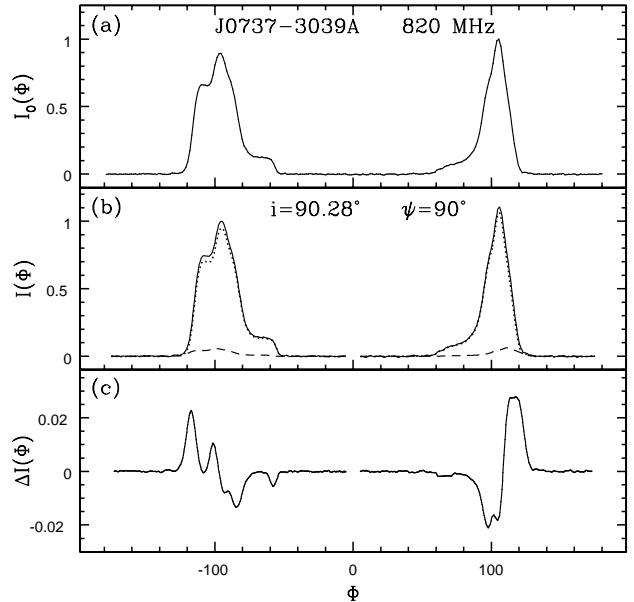


Fig. 5. | (a) Pulse profile of J0737-3039A far from conjunction,  $I_0(\Phi)$ . (b) Contributions to the total pulse profile  $I(\Phi)$  (solid curve) at conjunction ( $\chi = 90^\circ$ ) due to the positive (dotted curve) and negative lensed images (dashed curve) taking into account different time delays and magnifications of the images. In the calculation  $i = 90.28^\circ$ ,  $\lambda = 50^\circ$ ,  $\chi = 45^\circ$ , and  $\Delta \lambda = 4^\circ$  are assumed. (c) Difference between  $I(\Phi)$  and  $I_0(\Phi)$ , with the latter magnified by  $A_+ + A_-$  and shifted by  $t_+$  in time at conjunction. The remaining residuals are due to the improperly subtracted negative image and are rather small. The flux units in the three panels are the same.

displacement of the image from the source is  $R$ , as given by eq. (3), and the image magnification  $A$  given by eq. (12). While aberration affects the arrival time of both images in the same way, lensing breaks this degeneracy and separates the arrival times of two weighted replicas of the unperturbed pulse profile. Assuming that in the absence of orbital motion and lensing the pulse profile is given by  $I(\Phi)$ , we find that the observed pulse profile at orbital phase  $\chi$ , including the light bending effect, is

$$I(\chi) = A_+ e^{i \chi} I_0(\chi - p - t_+) + A_- e^{-i \chi} I_0(\chi - p + t_-); \quad (24)$$

where the factors  $e^{\pm i \chi}$  accounts for the absorption of pulsar signal by plasma in the magnetosphere of companion. The time delays  $t$  for both images include not only the rotational contributions [eqs. (8), (10), (21) and (23)], but also the geometric delay and the (modified) Shapiro delay (see Lai & Raikov 2005). Note that  $A$ ,  $p$ ,  $t$  are all functions of the orbital phase  $\chi$ .

For illustrative purposes, we assume  $A_+ = 1$ , and show in Figure 5 the relative contributions of the two images in shaping the pulse profile  $I(\Phi)$  near the orbital conjunction for  $i = 90.28^\circ$ . In practice, one could adopt a simple procedure when analyzing arrival times near conjunction: since the  $A_+$  image dominates the lightcurve, one would naturally assume that the timing residual due to lensing is primarily given by  $t_+$  and the negative image contributes to the pulse profile mainly through its magnification. Figure 5c depicts the relative error

incurred by this assumption: we plot the difference between  $I_0$  magnified by  $A_+ + A_-$  and shifted by  $t_+$  in time and the real profile  $I(\tau)$  which properly includes contributions from both images at conjunction. One can see that this simple procedure does perform quite well, and the flux residuals due to improper subtraction of the negative image are at most several percent. In reality, since the light of “+” image passes closer to the companion star than the light of “-” image, and the magnetoospheric absorption depends strongly on the plasma density, we expect that near conjunction,  $I_+$  is much greater than  $I_-$ . This would further decrease the contribution of the “-” image to the distortion of the pulse profile.

#### 4. detectability of rotational delays and pulse distortion

The rotational time delays discussed in previous sections could be observed in different ways. The aberration effect results in arrival time variation and pulse distortion throughout the whole cycle of the orbital motion, while the lensing effect is important only in very edge-on systems near the superior conjunction of the pulsar. As discussed above, the pulse profile and polarization of PSR J0737-3039A imply that our line of sight crosses the edge of the pulsar’s emission cone (Demorest et al. 2004), resulting in significant pulse distortion and the associated latitudinal delay. For example, taking  $\Omega = 50$ ,  $\tan i_0 = 0.08$  and  $i = 90.28^\circ$ , we find, for the aberration delays,  $A = 4.7 \sin i$  s,  $B = -0.023 \cos i$  s,  $C = 59 \cos i$  s and  $D = 0.3 \sin i$  s. The lensing delays are shown in Figures 1 and 2. Aberration results in fractional pulse width variation of order  $\delta = \delta_0 = p(t_A^{\text{lat}}) = 0$ ,  $pC = 0$ ,  $10^2 \cos i$  in the course of the pulsar’s orbital motion. For a few seconds around the superior conjunction, light bending gives rise to additional profile distortion at a similar level.

Motivated by our results, we propose to perform timing of separate components of the pulse profile to detect pulse dilation/contraction and the associated latitudinal delays. Instead of fitting one template to the whole observed pulse profile to determine its overall timing displacement (or the arrival time of the pulse centroid), one can directly fit templates for each individual component of the profile. Assuming that some pairs of components represent the leading and trailing edges of the emission cone through our line of sight, one can measure the difference between their times of arrival and correlate its variation with the orbital phase. This method presents a relatively easy way of measuring the latitudinal delays and extracting pulsar parameters from them. In the case of PSR J0737-3039A, periodic profile distortions must be very strong because of the small ( $4^\circ$ ) magnetic inclination angle of pulsar A with respect to its spin (Demorest et al. 2004). The latitudinal delay is of order  $C = 59 \cos i$  s, which should be detectable since RMS timing residuals of pulsar A are already at the level of 27 s (Lyne et al. 2004). Such detection would directly constrain  $\Omega$ ,  $i$  and  $\Omega$ .

Detection of the standard “longitudinal” aberration delay (eqs. [8]-[9]) is a more difficult task. Damour & Dehnen (1986) were the first to recognize that this delay cannot be observed directly as a timing variation on the orbital time scale since it can be fully absorbed into

the Roemer delay by rescaling/redesigning the eccentricity, semimajor axis, epoch of periastron and two other post-Newtonian parameters. More precisely, because of the aberration delay, the observed values of the semimajor axis  $a^{\text{obs}}$ , eccentricity  $e^{\text{obs}}$ , and the epoch of periastron  $T_0^{\text{obs}}$  are related to the true values of these quantities  $a^{\text{true}}$ ,  $e^{\text{true}}$ ,  $T_0^{\text{true}}$  by the formulae

$$\frac{a^{\text{obs}}}{a^{\text{true}}} = \frac{e^{\text{obs}}}{e^{\text{true}}} = 1 + \frac{1}{1};$$

$$1 \frac{cA}{a_p \sin i} = 3.3 \cdot 10^6 \sin i; \quad (25)$$

$$T_0^{\text{obs}} = T_0^{\text{true}} \frac{p}{1 - e^2} \frac{1}{b} \frac{1}{2};$$

$$2 \frac{cB}{a_p \sin i} = 1.6 \cdot 10^8 \cos i; \quad (26)$$

where the numbers are for the J0737-3039 system. The degeneracy with Roemer delay implies that to detect aberration delay one must look for arrival time variation over longer timescales. As a result of geodetic precession, both angles  $\Omega$  and  $i$ , and thus  $a^{\text{obs}}$ ,  $e^{\text{obs}}$ ,  $T_0^{\text{obs}}$  will change with amplitude  $\frac{1}{1}$ , on the timescale of the precession period. In some systems the precession can be rather rapid (with period of tens of years) and, if  $\frac{1}{1}$ ,  $\frac{2}{2}$  are not too small, this variation can be detected in long-term observations and the pulsar spin orientation can be inferred (Stairs et al. 2004). In the case of the PSR J0737-3039 system, the precession period of pulsar A is 75 yr, and the relative variation of observed eccentricity and semimajor axis on this timescale is  $3.3 \cdot 10^6 \sin i$ , while the observed epoch of periastron varies by 22 s. The current timing accuracy of J0737-3039A (Stairs 2005, private communication) allows determination of  $e^{\text{obs}}$  and  $a^{\text{obs}}$  with relative accuracy of  $1.7 \cdot 10^5$  and  $1.4 \cdot 10^6$ , respectively, and the measurement of  $T_0^{\text{obs}}$  has absolute accuracy of 35 ms. Thus, it would in principle be possible to detect variation of  $a^{\text{obs}}$  (but not of  $e^{\text{obs}}$  or  $T_0^{\text{obs}}$ ) caused by geodetic precession and longitudinal aberration at a 2 level after tens of years of timing observation.

Much better measurement can be made if one monitors the long-term drift of timing positions of individual pulse features instead of the whole profile. Then the amplitude of drift<sup>8</sup> in  $a^{\text{obs}}$ ,  $e^{\text{obs}}$ ,  $T_0^{\text{obs}}$  caused by geodetic precession is augmented by the much more significant latitudinal aberration. Since the latitudinal delay has the same dependence on the orbital elements as the longitudinal one, its effect on variation of  $a^{\text{obs}}$ ,  $e^{\text{obs}}$ ,  $T_0^{\text{obs}}$  can be included by simply changing  $A = A + C$  and  $B = B + D$  in (25) and (26). As a result,  $a^{\text{obs}}$  and  $e^{\text{obs}}$  determined from timing of individual pulse features vary on geodetic precession timescale with relative amplitude  $4.2 \cdot 10^5 (\cos i + 0.08 \sin i)$ . This should give a highly significant detection of geodetic variation of  $a^{\text{obs}}$  (and on a shorter baseline than the longitudinal aberration variation) and yield a measurement of  $e^{\text{obs}}$  variation at a 2 level. The accompanying variation of  $T_0^{\text{obs}}$  at the level of 0.4 ms would still escape detection.

Time delays caused by gravitational light bending do not suffer from the degeneracy with Roemer delay because of their unique time dependence (see eqs. [10], [23],

<sup>8</sup> In this approach the orbital parameters should be determined separately for each pulse component.

and Figs. 1-2). As noted before, in general the rotational lensing delay is asymmetric with respect to the conjunction, which may facilitate the separation of this delay from the geometric delay and the (corrected) Shapiro delay (Lai & Radev 2005). For the parameters adopted in Figure 1, the maximum amplitude of  $(\Delta t)_L$  for the positive inage is 5 s (for  $i = 90^\circ 28'$  or the minimum  $R_s = 4000$  km), while  $(\Delta t)_L^{(lat)}$  reaches as high as 70 s, both achieved within several seconds of conjunction. The latter delay would be detectable if one times the arrival of individual features of the pulse profile.

Detecting the lensing-related time delays may be a challenging task. One factor which limits the accuracy of pulsar timing arises from the intrinsic variation of the pulse profile from one pulse to the next. If one times the arrival of a pulse feature with width  $w$ , then the timing accuracy after combining  $N_p$  pulses is  $\Delta t = \frac{w}{N_p}$ . For PSR J0737-3039A, the pulse has two peaks, each with width  $w = 4$  ms. The lensing effect lasts about 4 s, so that in each orbit there are  $N_p = 200$  pulses during the lensing event, and about half of them<sup>9</sup> may be used for timing purposes. This gives  $\Delta t = 0.4$  ms for a single passage through conjunction, somewhat larger than the amplitude of  $(\Delta t)_L^{(lat)}$  (for  $i = 90^\circ 29'$ ). By adding up pulses from many orbits one will obtain better timing accuracy which may make the detection of  $(\Delta t)_L^{(lat)}$  possible. This would set a robust constraint on the system's inclination angle.

Finally, all rotationale effects (both aberration and lensing) that we described in application to J0737-3039A should also be relevant for J0737-3039B. Since the masses of the two pulsars are quite similar, the variation of the direction of emission vector  $\mathbf{N}$  is also similar for both pulsars, but the spin period of pulsar B,  $P_B = 2.8$  s is significantly longer than  $P_A = 23$  ms. As a result, the amplitudes of all spin-dependent delays for pulsar B are

10<sup>8</sup> higher than for pulsar A. However, the current timing accuracy of pulsar B, 2.7 ms (Lyne et al. 2004), is much poorer than that of pulsar A. The pulse profile of pulsar B is unstable and subject to variations throughout the orbit, presumably due to the influence of the intense wind/radiation from pulsar A (Ramachandran et al. 2004) Moreover, the spin and magnetic geometry of pulsar B (not wellconstrained observationally at present) may not be very favorable for exhibition of large latitudinal effects<sup>10</sup>.

## 5. discussion

Pulse profile distortion associated with the latitudinal aberration delay is the most easily measurable among all

<sup>9</sup> Lensing effects manifest themselves only very near the conjunction (when  $R_s \approx R_E$ ) where absorption by magnetospheric plasma of pulsar B is important (Kaspi et al. 2004; Radev & Goldreich 2004). At the same time, McLaughlin et al. (2004) and Lyutikov & Thompson (2005) have demonstrated that even very close to A's superior conjunction radio signal of A can still pass through B's magnetosphere almost unattenuated at some intervals of B's rotation phase within which at least several rotational periods of A can be detected. It is this penetrating part of A's radio flux that can be used to search for gravitational lensing effects in J0737-3039.

<sup>10</sup> A detailed modeling of the modulation of the pulsar A eclipse by pulsar B's rotation yields the following parameters for pulsar B: the angle between the spin axis and magnetic axis  $75^\circ$ , the inclination of the spin axis to the orbital angular momentum axis  $60^\circ$  (Lyutikov & Thompson 2005).

rotational timing effects in J0737-3039A. Its large magnitude is a direct consequence of the specific spin-magnetic orientation of the pulsar as inferred by Demorest et al. (2004). This effect should be detectable with the current timing accuracy if the arrival times of individual pulse component (rather than the pulse centroid) are monitored. However, if this effect is not found in the data, we can suggest two possible reasons. First, it is conceivable that at the present time the spin orientation is such that  $\cos i \approx 1$ , resulting in a rather small profile distortion by aberration (see eq. [22]). However, such a situation would not last since geodetic precession of the pulsar spin axis changes on the timescale of years. There is also a pathological possibility that the spin of pulsar A is almost aligned with the orbital angular momentum which, because of the edge-on orientation of the system, would naturally make  $\cos i \approx 1$ . This would account for the remarkable stability of J0737-3039A pulse profile (Manchester et al. 2005), but it would require a very large opening angle of the emission cone,  $\approx 90^\circ$ , which seems unlikely. Second, it is possible that the spin and magnetic orientations inferred by Demorest et al. (2004) are incorrect, e.g. because of the failure of RVM. This would not be very surprising given that the polarization data are corrupted by quasi-orthogonal modes. Even the interpretation of the emission as coming from a single magnetic pole can be called into question. If this were the case, the angles  $\alpha$  and  $\beta$  could be different from what we used in our estimates, possibly reducing the magnitude of pulse distortion. Thus, measuring the pulse variation in J0737-3039A on the orbital timescale can be used to probe the emission and spin geometry of pulsar A.

Pulse shape variations caused by latitudinal shifts are very promising from the observational point of view: unlike the lensing effects, profile dilation due to orbital aberration does not require special orientation of orbital plane which makes it potentially observable in many binary systems. As far as we are aware, no one has attempted to detect pulse profile expansion/contraction of the predicted form correlated with the phase of pulsar orbital motion. The only possible exception is the study of PSR B1534+12 by Stairs et al. (2004) in which pulse shape variations were detected through subtraction of a template profile from the observed pulse profile. Residuals of profile intensity were quantified and their secular change was ascribed to geodetic precession of pulsar spin in the gravitational field of its companion. A less significant change of residuals was also detected on the orbital timescale which allowed Stairs et al. to determine pulsar spin orientation free from assumptions about the beam geometry. This procedure seems to be less straightforward than a direct measurement of the variation of the phase separation between different pulse components that we propose to perform.

It may be possible to infer the PSR J0737-3039A spin orientation from rotationale effects alone, without resorting to polarimetric observations. The pulse profile variations on the orbital timescale and the long-term geodetic variations of orbital parameters may be enough to measure A's spin orientation with respect to its magnetic axis (angle  $\alpha$ ) and with respect to orbital angular momentum of the binary. Detection of lensing effects would additionally refine the accuracy of such measurement and

may help verify the assumption of circular beam shape. Rotational delays may be measurable in other compact binary pulsar systems with significant  $v=c$ . In such systems pulse profile variations on orbital timescales may be a telltale signature of latitudinal aberration. The effect is strongest for pulsars in which the polarization angle of radio signal does not exhibit significant variation across the pulse profile, implying small value of  $\tan \alpha$  and large  $\alpha$  (see eq. [18]). This could serve as a useful criterion for selecting potential targets to detect orbital pulse profile variations (geodetic variations will also be enhanced for such pulsars by latitudinal effects, see §4). Timing of individual pulse components needed for such detection should be facilitated in pulsars with rich pulse profiles exhibiting many symmetric sharp features. Using

<sup>11</sup> Time interval during which such observations are taken must be small compared to the geodetic precession period since otherwise

this technique to measure pulsar orientation with high significance may require stacking together observations obtained in many orbits<sup>11</sup>, but, presumably, this would still require much shorter baseline than is needed for detection of geodetic precession.

We thank Jim Cordes and Ingrid Stairs for useful discussion and Vicki Kaspi and René Breton for making data on pulse profile of J0737-3039A available to us. RR R thankfully acknowledges the financial support by the W.M. Keck Foundation and NSF via grant PHY-0070928. DL thanks CITA and TAIARA (Taiwan) for hospitality and is supported in part by NSF grant AST 0307252 and NASA grant NAG 5-12034.

system's geometry would change.

#### REFERENCES

- Arons, J., Backer, D. C., Spitkovsky, A., & Kaspi, V. 2004, in *Binary Radio Pulsars*, ASP Conf. Series; eds. F. A. Rasio & I. H. Stairs (astro-ph/0404159)
- Blundell, R. & Teukolsky, S. A. 1976, *ApJ*, 205, 580
- Burgay, M., D'Amico, N., Possenti, A. et al. 2003, *Nature*, 426, 531
- Coles, W. A., McLaughlin, M. A., Rickett, B. J. et al. 2004, *ApJ*, in press (astro-ph/0409204)
- Damour, T. & Deruelle, N. 1986, *Ann. Inst. Henri Poincaré*, 44, 263
- Demorest, P. et al. 2004, *ApJ*, 615, L137
- Doroshenko, O. V. & Kopeikin, S. M. 1995, *MNRAS*, 274, 1029
- Góicoechea, L. J. et al. 1995, *A&A*, 303, 502
- Kaspi, V., Ransom, S., Backer, D. C. et al. 2004, *ApJ*, 613, L137
- Komesarov, M. M. 1970, *Nature*, 225, 612
- Kramer, M., Xilouris, K. M., Lorimer, D. R., Doroshenko, O., Jessner, A., Wielebinski, R., Wolszczan, A., & Camilo, F. 1998, *ApJ*, 501, 270
- Lai, D. & Rakhov, R. R. 2004, *ApJ*, 621, 41L
- Lyne, A. G. et al. 2004, *Science*, 303, 1153
- Lyutikov, M. & Thompson, C. 2005, *ApJ*, submitted (astro-ph/0502333)
- Manchester, R. N. et al. 2005, *ApJ*, in press (astro-ph/0501665)
- McLaughlin, M. A. et al. 2004, *ApJ*, 613, L57
- Radhakrishnan, V. & Cooke, D. 1969, *ApL*, 3, 225
- Rakhov, R. R., & Goldreich, P. 2004, *ApJ*, submitted (astro-ph/0412355)
- Ramachandran, R., Backer, D. C., Demorest, P., Ransom, S., & Kaspi, V. 2004, astro-ph/0404392
- Rankin, J. M. 1993, *ApJ*, 405, 285
- Ransom, S. et al. 2004, *ApJ*, 609, L71
- Schneider, J. 1990, *A&A*, 232, 62
- Smarr, L. L. & Blundell, R. 1976, *ApJ*, 207, 574
- Weisberg, J. M. & Taylor, J. H. 2002, *ApJ*, 576, 942